Developmental Cell, Vol. 4, 307–319, March, 2003, Copyright ©2003 by Cell Press

Drosophila gurken (TGFα) mRNA Localizes as Particles that Move within the Oocyte in Two Dynein-Dependent Steps

Nina MacDougall, Alejandra Clark, Eilidh MacDougall, and Ilan Davis*
Wellcome Trust Centre for Cell Biology
ICMB
King's Buildings
University of Edinburgh
Mayfield Road
Edinburgh EH9 3JR
Scotland
United Kingdom

Summary

In *Drosophila* oocytes, *gurken* mRNA localization orientates the TGF-α signal to establish the anteroposterior and dorsoventral axes. We have elucidated the path and mechanism of *gurken* mRNA localization by time-lapse cinematography of injected fluorescent transcripts in living oocytes. *gurken* RNA assembles into particles that move in two distinct steps, both requiring microtubules and cytoplasmic Dynein. *gurken* particles first move toward the anterior and then turn and move dorsally toward the oocyte nucleus. We present evidence suggesting that the two steps of *gurken* RNA transport occur on distinct arrays of microtubules. Such distinct microtubule networks could provide a general mechanism for one motor to transport different cargos to distinct subcellular destinations.

Introduction

mRNA localization provides an efficient posttranscriptional method of targeting many kinds of proteins to their sites of function in a wide range of organisms (Jansen, 2001; Kloc et al., 2002; Lipshitz and Smibert, 2000; Palacios and Johnston, 2001). In a variety of cases, mRNA localization is thought to involve polarized transport of mRNA by cytoskeletal motors (Tekotte and Davis, 2002). However, only in a few cases has transport been demonstrated by real-time imaging of directed movement of RNA. For example, *ASH1* mRNA localizes to the buds of dividing yeast cells, thus suppressing mating-type switching in the daughter cell (Bobola et al., 1996). The movement of *ASH1* mRNA indirectly tagged with GFP has been visualized directly (Bertrand et al., 1998) and requires Myosin V and actin. She2 and She3 act as linkers between Myosin and the RNA (Jansen et al., 1996; Long et al., 2000; Munchow et al., 1999; Takizawa and Vale, 2000). In the *Drosophila* blastoderm embryo, *wingless* (*wg*) and pair-rule apical transport of RNA particles has been visualized directly with injected fluorescently labeled RNA. Apical transcript localization in the embryo requires cytoplasmic Dynein (Dynein), the major minus end-directed microtubule (MT) motor (Wilkie and Davis, 2001). Egalitarian (Egl) and Bicaudal-D (BicD) may act as linkers between pair-rule RNA and the Dynein motor complex (Bullock and Ish-Horowicz, 2001).

In *Drosophila* oocytes, mRNA localization plays a central role in axis specification, but the role of cytoskeletal motor proteins has not been tested directly by observation of the movement of mRNA. The embryonic axes are preformed during oogenesis through the sorting of different mRNAs to distinct regions of the oocyte (Jansen, 2001). *gurken* (*grk*) mRNA localization plays a key role in breaking the initial symmetry of the oocyte by restricting the Grk-transforming growth factor-α (TGF-α) signal to particular groups of overlying follicle cells (Gonzalez-Reyes et al., 1995; Neuman-Silberberg and Schüpbach, 1993). There are two rounds of Grk signals at different times during oogenesis, both of which are received by Torpedo, an EGF receptor in the follicle cells (Nilson and Schüpbach, 1999). In stage 6, *grk* mRNA and Grk protein are localized at the posterior of the oocyte, thus instructing a group of follicle cells to become posterior in identity. These cells then send a signal back to the oocyte that initiated the formation of the anteroposterior axis. The signal leads to the repolarization of the oocyte MTs and the migration of the oocyte nucleus to the dorsoanterior corner of the oocyte (Gonzalez-Reyes and St Johnston, 1998). Before stage 7 an MT-organizing center (MTOC) is located at the posterior of the oocyte, the site at which most MT minus ends are localized (Clark et al., 1994, 1997; Micklem et al., 1997; Theurkauf et al., 1992). By stage 8, the posterior MTOC disassembles and a diffuse MTOC forms in the anterior. The anterior MTOC has been visualized with Nod-LacZ, a putative MT minus end marker (Clark et al., 1997), and Centrosomin, a centrosome component (Brendza et al., 2000), as well as the MT-nucleating components, γ-Tubulin37C (γTub37C) and γ-Tubulin ring complex protein 75 (Dgrip75) (Schnorrer et al., 2002). Plus ends of MTs, visualized with Kinesin-LacZ (Kin-LacZ), are found at the posterior of the oocyte (Clark et al., 1994). This results in an anteroposterior gradient of MT concentration, with the highest concentration at the anterior, which has been visualized with Tau-GFP (Micklem et al., 1997), a fusion containing the MT binding protein Tau. The second round of Grk signaling initiates dorsoventral axis formation in stage 9, when *grk* mRNA and protein are localized in an anterodorsal cap near the oocyte nucleus. The overlying dorsal follicle cells are instructed by the Grk signal to adopt dorsal fates, leading later to secretion of correct eggshell structures, such as the dorsal appendages (Nilson and Schüpbach, 1999; van Eeden and St Johnston, 1999).

The breaking of the initial axial symmetry of the oocyte involves several other localized transcripts in addition to *grk*. *bicoid* (*bcd*) mRNA is localized to the extreme anterior cortex of the oocyte, leading to a morphogenetic gradient of Bcd protein when it is translated in the embryo (Driever and Nüsslein-Volhard, 1988). *oskar* (*osk*) mRNA is localized at the extreme most-posterior part of the oocyte and embryo and specifies the future

*Correspondence: ilan.davis@ed.ac.uk

germ cells and posterior structures through recruitment of many other localized posterior components by the Osk protein (Ephrussi et al., 1991). While the functions of *grk*, *bcd*, and *osk* have been studied in detail, the mechanism of localization of these transcripts is not as well understood (Tekotte and Davis, 2002). *osk* mRNA localization to the posterior requires actin and Tropomyosin, probably for anchoring at the posterior (Erdelyi et al., 1995), a crucial step in pole plasm assembly (Vanzo and Ephrussi, 2002). The MT plus end motor, Kinesin I (Kin I), is probably required for transport of *osk* mRNA along MTs to their plus ends (Brendza et al., 2000), for its exclusion from the lateral cortex (Cha et al., 2001), and for all cytoplasmic movements in the oocyte (Palacios and Johnston, 2002). *osk* mRNA localization is also likely to require cytoplasmic movements to deliver it to the posterior (Glotzer et al., 1997). Surprisingly, Kin light chain is not required for this process (Palacios and Johnston, 2002). However, the path of movement of *osk* mRNA has not been visualized directly either in wild-type or Kin mutants. *bcd* mRNA localization to the anterior requires Swa, which interacts with Dynein in yeast two-hybrid assays (Schnorrer et al., 2000), but the role of Dynein in *bcd* mRNA localization has not yet been tested directly. *bcd* localization also requires Exu protein (St Johnston et al., 1989) for the correct path of localization of injected *bcd* RNA in living oocytes (Cha et al., 2001). Exu-GFP fusion protein has been visualized in particles that move within the oocyte (Theurkauf and Hazelrigg, 1998), but it remains unclear whether Exu and *bcd* mRNA coassemble in the same particles (Wilhelm et al., 2000).

In comparison with *bcd* and *osk*, less is known about the mechanism of localization of *grk* mRNA within the oocyte. Like *bcd* and *osk*, *grk* mRNA may be transcribed at early stages in nurse cells (Thio et al., 2000), but, in later stages, *grk* mRNA may be transcribed in the oocyte nucleus (Saunders and Cohen, 1999). *grk* mRNA localization requires MTs (Pokrywka and Stephenson, 1991). Kin I is required for the localization of *grk* mRNA to the dorsoanterior corner, possibly because of a requirement to recycle Dynein back to the posterior (Brendza et al., 2002). Overexpression of p50/dynamytin, a subunit of the dynactin complex that is required for Dynein processivity (King and Schroer, 2000), disrupts *grk* RNA localization, suggesting a possible role for Dynein in *grk* mRNA localization (Januschke et al., 2002). However, as in the cases of *bcd* and *osk* mRNAs, the path of *grk* mRNA has not been defined, and it has not been tested directly whether Dynactin, Dynein, and Kinesin are required for active transport of *grk* as opposed to cytoplasmic streaming or diffusion and for the anchoring of *grk* or a factor required for its localization.

Here, we have observed the path of movement and elucidated the mechanism of *grk* RNA localization in the oocyte by studying its movement in real-time in living egg chambers. Injected *grk* RNA assembles into discrete particles that move first to the anterior cortex and then turn and move dorsally toward the oocyte nucleus. Both steps involve transport to the minus ends of MTs mediated by Dynein. We propose and show some supporting evidence for the view that the two steps of *grk* movement take place on two distinct arrays of MTs, the first orientated toward the anterior and the second associated with the oocyte nucleus.

Results

Injected *grk* Transcripts Localize in Cultured Egg Chambers like Endogenous *grk* mRNA to the Anterodorsal Corner of the Oocyte

To investigate the path and mechanism of *grk* mRNA localization, we developed a rapid real-time injection assay for *grk* RNA localization in living oocytes cultured in oxygen-rich halocarbon oil. About 1 hr after injection, fluorescently labeled *grk* transcripts localize to a very similar site to the endogenous transcripts. The assay is based on previous procedures used to inject fluorescently labeled mRNA into embryos (Bullock and Ish-Horowicz, 2001; Wilkie and Davis, 2001) and on our modifications of previous methods used to inject mRNA into living egg chambers or embryos (Glotzer et al., 1997; Lall et al., 1999). We used time-lapse cinematography with low-powered objectives to capture the movement and localization of *grk* RNA over the entire oocyte (Experimental Procedures).

In stage 8 of oogenesis, endogenous *grk* transcripts are localized in the oocyte in an anterior ring with an enrichment at the dorsoanterior corner near the oocyte nucleus. By early stage 9 the majority of *grk* RNA is located in the dorsoanterior corner, with a small amount present in the entire anterior region. Fluorescently labeled *grk* RNA injected into oocytes of stage 8–10B egg chambers is correctly localized in 81% of cases ($n = 96$). Localization efficiency is higher in stages 8–9 (87%, $n = 47$) and stage 10A (83%, $n = 35$) than in stage10B (57%, $n = 14$). *grk* transcripts localize correctly approximately 1 hr after injection into any part of the oocyte, including the extreme posterior end (Figures 1A–1F).

The time-lapse movies we captured suggest that the localization of *grk* RNA occurs in two steps (Figure 1 and Supplemental Movie S1 at http://www.developmentalcell.com/cgi/content/full/4/3/307/DC1). The RNA begins to move toward the anterior soon after its injection (Figure 1B). Thirty minutes after injection, the RNA is strongly localized along the entire anterior but begins to be enriched at the dorsoanterior corner (Figure 1C). Between 30 and 60 min after injection, *grk* RNA becomes progressively much more concentrated in the dorsoanterior corner, and the anterior signal is diminished (Figure 1D). These results suggest that *grk* mRNA first moves to the anterior and then to the dorsoanterior corner, rather than being degraded everywhere other than at the dorsoanterior corner. In contrast, we find that injected fluorescent *bcd* RNA fails to correctly localize to the anterior cortex when injected into the oocyte (data not shown), in agreement with previous studies (Cha et al., 2001). We conclude that, unlike for *bcd*, all the machinery required for *grk* mRNA localization is present within the oocyte cytoplasm.

In addition to localizing at the dorsoanterior corner, injected *grk* RNA also accumulates at a lower level in the opposite side of the oocyte, at the ventroanterior corner (Figures 1E and 1F). To determine whether this additional site of localization is also found in the case of endogenous *grk* mRNA, we used high-resolution fluorescent in situ hybridization methods (Wilkie et al, 1999; Wilkie and Davis, 2001) (detailed protocol available by

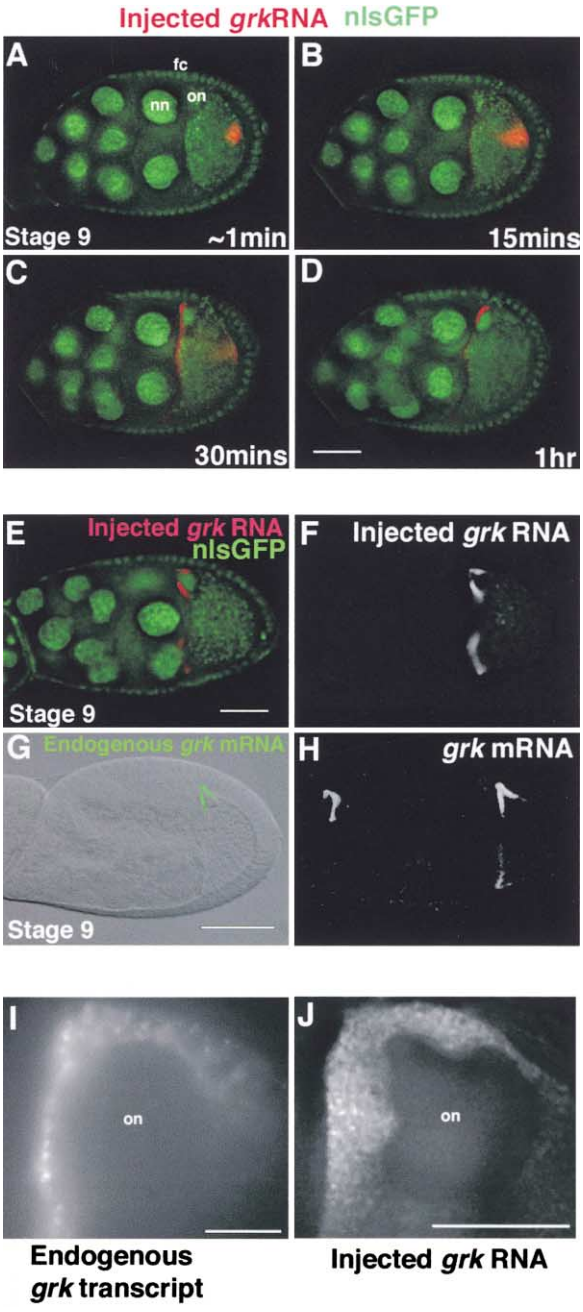

Figure 1. Injected *grk* RNA, like Endogenous *grk* Transcripts, Localizes to the Dorsoanterior Corner of the Oocyte

(A–D) Time-lapse movie of the movement of injected Alexa Fluor 546-UTP-labeled *grk* RNA in a living stage 9 egg chamber expressing nlsGFP.

(A) One minute after the injection of the *grk* RNA in the posterior of the oocyte. fc, follicle cells; nn, nurse cell nuclei; on, oocyte nucleus.

(B) Fifteen minutes after the injection, the RNA has begun to move toward the anterior.

(C) Thirty minutes after the injection, much of the RNA is localized to the anterior of the oocyte.

(D) One hour after the injection, the RNA is predominantly localized at the dorsoanterior cap.

(E–H) Stage 9 egg chambers showing a comparison of the final distribution of injected *grk* RNA and endogenous *grk* transcripts. In both cases, the majority of the RNA has accumulated at the oocyte nucleus, and a fraction of the RNA has accumulated at the ventroanterior corner.

(E and F) Living stage 9 egg chamber injected with *grk* RNA.

(G and H) Endogenous *grk* transcripts visualized by in situ hybridization in a fixed stage 9 egg chamber.

(I and J) High-magnification comparison of the distribution of injected *grk* RNA and endogenous *grk* transcripts showing that both are localized in a punctate manner in a dorsoanterior cap around the oocyte nucleus (on). The scale bars represent 50 μm in lower-powered images and 10 μm in high-powered images in this and all other figures. In this and all subsequent figures, the oocyte is orientated with dorsal up and posterior to the right, unless otherwise stated.

request) and three-dimensional imaging of entire fixed egg chambers (Davis, 2000). We modified the in situ procedure to allow greater probe penetration and increased signal to noise ratio (Experimental Procedures). In stage 9 egg chambers, endogenous *grk* mRNA shows a pattern of accumulation very similar to that of the injected RNA, with the majority of the RNA in a dorsoanterior cap and some RNA concentrated in the ventroanterior corner (Figures 1G and 1H). The translation of the ventroanterior RNA is presumably repressed. We also found that high-resolution imaging of endogenous *grk* transcripts and injected *grk* RNA showed that both are localized in a punctate pattern in the dorsoanterior corner (Figures 1I and 1J). We conclude that injected *grk* RNA localizes to the same site as endogenous *grk* mRNA approximately 1 hr after injection.

To test whether *grk* is specific in its ability to localize to the dorsoanterior corner, we injected the anteriorly localized transcript, *fs(1)K10 (K10)*. A 44 nt *K10* small stem loop, previously shown to localize to the anterior region as a transgene in oocytes (Serano and Cohen, 1995) and apically when injected as part of a larger RNA into blastoderm embryos (Bullock and Ish-Horowicz, 2001), localizes anteriorly when injected into the oocyte, albeit less efficiently than *grk* RNA (26% anteriorly localized, 64% unlocalized, n = 15; Figure 2A). In contrast, a mutant *K10* stem loop previously shown not to localize as a transgene in oocytes and when injected into blastoderm embryos (Bullock and Ish-Horowicz, 2001; Serano and Cohen, 1995) fails to localize when injected into oocytes (0% anteriorly localized, n = 9; Figure 2B). In contrast, *hb* RNA, which is not normally found in the oocyte and is unlocalized in embryos (Davis and Ish-Horowicz, 1991), becomes evenly distributed when injected into the oocyte (0% localization, n = 12; Figure 2D). We conclude that the anterodorsal localization of injected *grk* RNA is specific.

Endogenous *grk* transcripts require the transacting protein Squid (*Drosophila* hnRNP A1) for correct anterodorsal localization (Kelley, 1993). We injected *grk* RNA into *squid* mutant egg chambers and found that injected *grk* RNA, like the endogenous transcripts, localizes to the entire anterior cortex, instead of the dorsoanterior corner (75% anteriorly localized, 25% unlocalized, n = 8; Figure 2C). In no case was injected *grk* RNA specifically enriched in the dorsoanterior corner of *squid* mutant oocytes. We conclude that our injection assay for *grk* RNA reflects faithfully the specificity of endogenous *grk* mRNA localization.

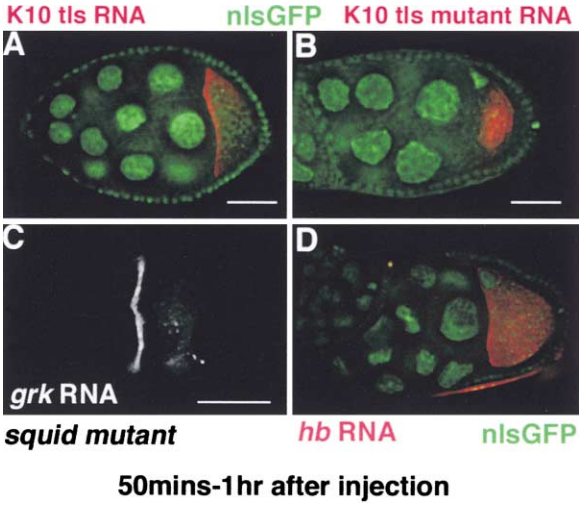

Figure 2. Dorsoanterior Localization of *grk* RNA Is Specific

(A) Stage 9 egg chamber injected with the *K10tls* (44 nt *K10* localization element). The RNA localizes to the anterior in 26% of injected oocytes.

(B) Stage 9 egg chamber injected with a mutated *K10tls* previously shown to disrupt localization. In all cases the RNA does not localize and remains near the injection site.

(C) Stage 9 *squid*^{1}/*Df(3)urd* oocyte injected with *grk* RNA. The RNA localizes tightly to the anterior and fails to form a dorsoanterior cap.

(D) Stage 9 egg chamber injected with *hb* RNA. *hb* RNA does not localize and diffuses throughout the ooplasm.

Injected *grk* RNA Assembles into Particles that Move in Two Phases

To determine the precise path of injected *grk* RNA movement, we imaged the movement of injected RNA in the oocyte at higher resolution at a time-lapse interval of one frame per second. Unlike in the blastoderm embryo, injected RNA in the oocyte appears diffuse at low resolution and moves with less well-defined directionality (Wilkie and Davis, 2001). However, by imaging at higher magnification and time resolution than in the embryo, we can readily resolve RNA into discrete particles that move in specific directions in the oocyte. These particle-tracking experiments confirm the two-step path of *grk* RNA localization observed with low-powered imaging. The RNA particles are usually apparent within 30–60 s of injection. Twenty-seven percent of the particles move in distinct, usually anterior or dorsal, paths in the plane of observation, 42% of the particles move rapidly into different focal planes and cannot be tracked, and the other 31% do not move substantial distances during the period of observation of 300 s (n = 265 particles) (Figure 3). Our observations suggest that all the particles eventually move to their correct destination, but, at any one time, particles go through periods of rapid motion interspersed by periods of stasis. During the periods of rapid motion, average speeds of 0.25 ± 0.013 μm/s and maximum speeds of 1.25 μm/s were observed. These speeds are approximately half of those observed in the embryo for *grk*, *wg*, and pair-rule RNA particle movements (this paper and Wilkie and Davis, 2001), probably because the particles pause more frequently in the oocyte than in the embryo. The speeds and paths taken by *grk* particles are entirely consistent with active transport, rather than diffusion and anchoring (Figure 3).

We were unable to track the particles at high resolution through their entire path of localization, as they eventually move out of the plane of focus and imaging at high power for long periods or through many focal sections causes an inhibition of the motility. This is probably due to photo-induced damage of the cellular machinery required for localization. Therefore, we were only able to image the movement of the RNA particles over short portions of their paths for 300 time points (5 min in total). Nevertheless, tracking the speed and direction of movement of many particles after injection of *grk* RNA at different sites in the oocyte has allowed us to reconstruct their entire route between the site of injection and their final destination.

To map the path of movement of *grk* RNA particles fully, we performed three kinds of particle-tracking experiments (Figure 3 and Supplemental Movies S2–S4 http://www.developmentalcell.com/cgi/content/full/4/3/307/DC1). In the first, we tracked the particles immediately after the injection of *grk* RNA in the center. In most cases, the particles move through the center toward the anterior of the oocyte (n = 214 particles; Figure 3A–3C), although, in some cases, the particles adopted diagonal routes directly to the oocyte nucleus. Unlike in *bcd* RNA injection experiments (Cha et al., 2001), we only sometimes observed particles moving toward the cortex (Figure 3B), and these appear to eventually move anteriorly from the cortex (data not shown). In the second type of particle-tracking experiment, we injected *grk* RNA in the center of the oocyte, waited for approximately 20 min, and then imaged the movement of particles at the anterior of the oocyte (n = 51; Figures 3D–3F). Near the anterior, some particles still move toward the anterior, while others move dorsally toward the nucleus. Interestingly, 11 particles were observed to move anteriorly, pause for a short period, and then make a sharp turn toward the dorsal corner (Figures 3E and 3F). In the third kind of particle-tracking experiment, we followed the movement of particles immediately after injection of *grk* RNA near the oocyte nucleus. In such experiments the oocyte was orientated with the dorsoanterior corner and nucleus uppermost, nearest the objective lens and out of focus. Particles near the oocyte nucleus generally move toward the nucleus (n = 17; Figures 3G–3I).

We plotted the angle of movement of the particles over their entire path (Figures 3J–3L). We found that, in the first particle-tracking experiment, the majority of particles moved toward the anterior (Figure 3J), and, in the second tracking experiment, the majority either moved anteriorly or dorsally (Figure 3K). In the third kind of particle-tracking experiment, the majority of the particles moved toward the oocyte nucleus (Figure 3L). To further test whether the turning of *grk* RNA particles we observe toward the dorsoanteriorly located nucleus is specific, we compared the direction of movement of *grk* particles in *squid* mutant and control egg chambers. In *squid* mutants *grk* RNA particles move less frequently to the dorsoanterior and more frequently to the ventral side than in controls (Figure 3M). We conclude that injected *grk* RNA and, by implication, endogenous *grk*

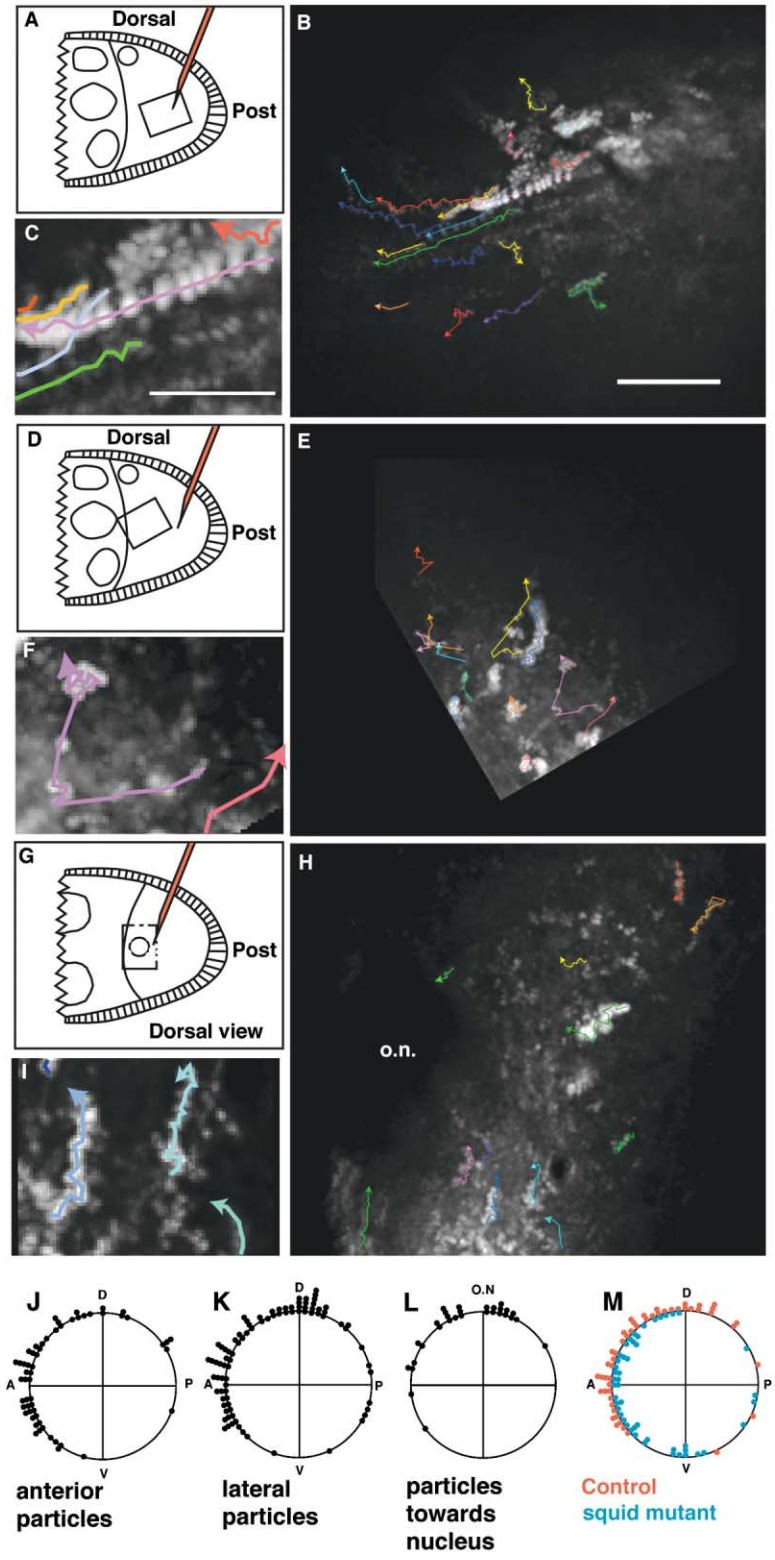

Figure 3. Injected *grk* RNA Assembles into Particles that Move First Anteriorly and then Dorsally Toward the Oocyte Nucleus

(A–C) The tracks of *grk* RNA particles and their direction of movement immediately after injection into the middle of the oocyte of a stage 9 egg chamber.

(A) Diagram showing the site of injection of *grk* RNA and orientation of the images acquired.

(B) Tracks of the path of movement of RNA particles identified by lines of various colors. The arrows indicate the direction of travel of the particles.

(C) An enlarged subregion of (B) showing some of the particles and their position over time.

(D) Diagram of another stage 9 egg chamber in which *grk* RNA was injected centrally into the oocyte.

(E) *grk* particles were allowed to move anteriorly for 30 min before their movement was tracked over time. Some particles travel anteriorly, but many travel dorsally (colored lines with arrows).

(F) An enlarged subregion of (E) showing a particle that travels in two phases, first anteriorly and then dorsally.

(G) Diagram of a stage 9 egg chamber in dorsal view (oocyte nucleus uppermost) injected with *grk* RNA in a broad region close to the oocyte nucleus.

(H) Particles close to the nucleus and their position and direction of movement over time (colored lines with arrows). Most particles move toward the oocyte nucleus.

(I) Enlargement of a subregion of (H) showing some particles moving toward the oocyte nucleus.

(J–L) Diagrams showing the direction of movement of *grk* RNA particles, illustrated as colored lines with arrows in (B), (E), and (H), respectively, and additional corresponding examples. The circles in (J) and (K) represent the angle of movement with respect to the four axes: D, dorsal; V, ventral; A, anterior; P, posterior. The circle in (L) represents the angle of movement relative to the oocyte nucleus (o.n.).

(J) Most particles move toward the anterior, some particles also move dorsally or anterodorsally, and a few move cortically.

(K) Most particles move dorsally or anteriorly, and a few moving cortically.

(L) Most particles move toward the oocyte nucleus.

(M) A comparison of the direction of movement of *grk* RNA particles in control (red) and *squid* (blue) mutant oocytes after injection halfway between the middle and the anterior of the oocytes. In the *squid* mutants most particles move anteriorly, but a few move dorsally or ventrally. In the control oocyte many particles move dorsally, but only one moves ventrally.

RNA become localized through an initial movement to the anterior through the center of the oocyte and then through a Squid-dependent dorsal movement from any part of the anterior toward the dorsoanterior corner.

grk mRNA Localization Requires MTs and Dynein

To investigate whether *grk* RNA localization requires an intact cytoskeleton, we coinjected or preinjected actin or MT inhibitors with *grk* RNA. Preinjection or coinjection

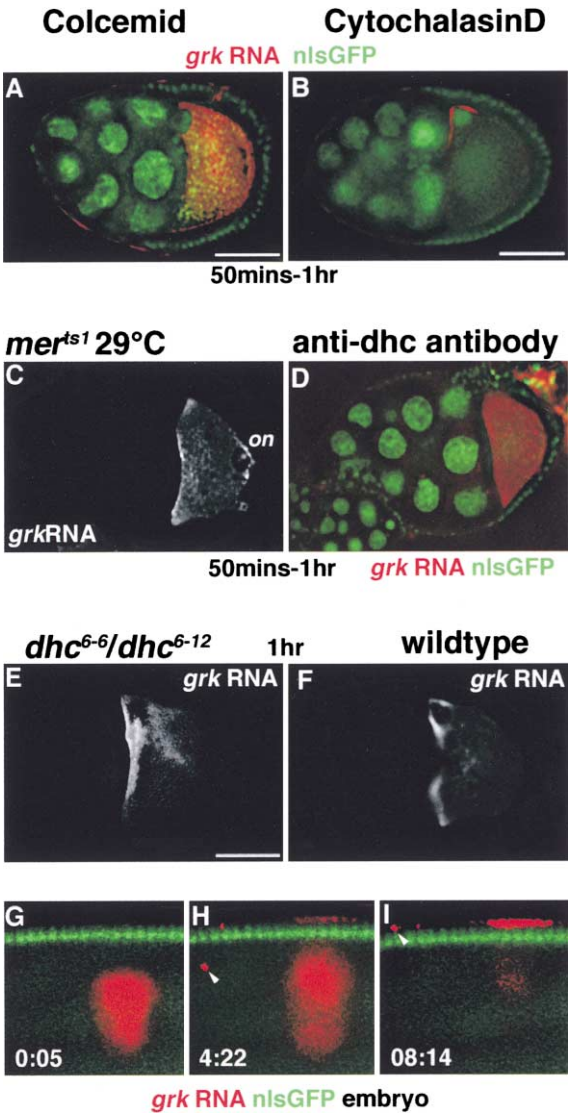

Figure 4. The First Step of *grk* RNA Localization Requires MTs and Dynein

(A) A stage 9 egg chamber 1 hr after coinjection of *grk* RNA and the MT-destabilizing drug, Colcemid (100 μg/ml). The RNA fails to localize within the oocyte.

(B) A stage 9 egg chamber 1 hr after coinjection of *grk* RNA and 150 μg/ml Cytochalasin D. *grk* RNA localizes to the dorsoanterior cap near the oocyte nucleus with normal kinetics.

(C) *merlin*^{ts1} mutant egg chamber 50 min after injection of *grk* RNA into the center of the oocyte. *grk* localizes to both the anterior and posterior of the oocyte, where minus ends of MTs are thought to localize. Note the oocyte nucleus at the posterior of the oocyte (on).

(D) A stage 9 egg chamber coinjected with *grk* RNA and P1H4 monoclonal anti-Dhc antibody (T. Hays). In all cases, *grk* RNA fails to localize within the oocyte.

(E) A stage 9 hypomorphic *dhc* mutant egg chamber injected with *grk* RNA, showing that the RNA is localized to the anterior after 1 hr (see text).

(F) A wild-type control egg chamber showing a strong dorsoanterior cap of *grk* RNA, 1 hr after injection.

(G–I) Time-lapse images of a living interphase 14 blastoderm embryo expressing nlsGFP fusion protein (green) and injected with *grk* RNA (red) at time 0. The time at which the images were captured after injection are shown in minutes and seconds in the bottom left hand corner of each panel. The arrowheads in (H) and (I) show an RNA particle, which formed from diffuse RNA at a second simultaneous site of injection of smaller quantities of RNA (not visible in [G]). In embryos, injected *grk* RNA localizes as particles with similar kinetics to *wg* and pair-rule RNA.

of Colcemid, an MT-depolymerizing drug, leads to an unlocalized distribution of *grk* RNA in the oocyte (100 μg/ml Colcemid, 0% localized, n = 26; 30 μg/ml Colcemid, 0% localized, n = 13; Figure 4A). In contrast, the actin-depolymerizing drug, Cytochalasin D, does not disrupt *grk* RNA localization to the dorsoanterior corner (86% localized, n = 15; Figure 4B). We conclude that *grk* RNA localization is dependent on intact MTs, but not on actin integrity.

To determine whether *grk* RNA localization is dependent on correct MT polarity, we injected *grk* RNA into *merlin* mutant egg chambers, which we previously showed fail to reorganize their MT at stage 7 of oogenesis (MacDougall et al., 2001). In *merlin* egg chambers, the posterior MTOC fails to disassemble and persists in later stages. In 50% of cases, the oocyte nucleus fails to migrate to the anterior and remains at the posterior of the oocyte. Our results show that, in *merlin* egg chambers, injected *grk* RNA localizes to the posterior near the misplaced oocyte nucleus, in addition to localizing along the entire anterior cortex (100% localized, n = 4; Figure 4C). We interpret these results as indicating that, in *merlin* mutants, the two steps of *grk* localization are disconnected, so that the RNA that completes the first step is not able to move from the anterior to the misplaced posterior nucleus, but the second step can occur in the absence of the first step. We conclude that *grk* mRNA localization depends on MT polarity and is normally targeted to minus ends of MTs at the anterior and near the oocyte nucleus.

The major minus end-directed MT-dependent motor in eukaryotic cells is Dynein. To test whether *grk* mRNA localization depends on Dynein, we injected *grk* RNA into egg chambers with reduced Dynein heavy chain (Dhc) activity. Dhc is the essential force-generating ATPase subunit of the large Dynein motor complex. Coinjection of either of two monoclonal antibodies against Dhc together with *grk* RNA is sufficient to completely inhibit the localization of *grk* RNA (0% localized, n = 34; Figure 4D), as is preinjection of either of the antibodies 10 min before *grk* RNA (data not shown). In contrast, injection of anti-Dynein antibody into Tau-GFP embryos does not alter the previously described (Micklem et al., 1997) anteroposterior gradient of MT (data not shown). Furthermore, injection of a control anti-HA antibody does not affect the localization of injected *grk* RNA (73% localized, n = 11). We conclude that a disruption of Dynein function by the anti-Dynein antibody is the cause of the inhibition of *grk* mRNA localization, rather than nonspecific effects of antibody injections or an indirect disruption of MT distribution.

We also studied the localization of injected *grk* RNA in hypomorphic semiviable *dhc* allelic combinations (Gepner et al., 1996). Injected *grk* RNA localizes more slowly in *dhc* mutant oocytes (Figures 4E and 4F). After 1 hr, 85% (n = 40) stage 9 wild-type oocytes injected with *grk* RNA were found to localize correctly in an anterodorsal cap near the nucleus. In contrast, only 21% of

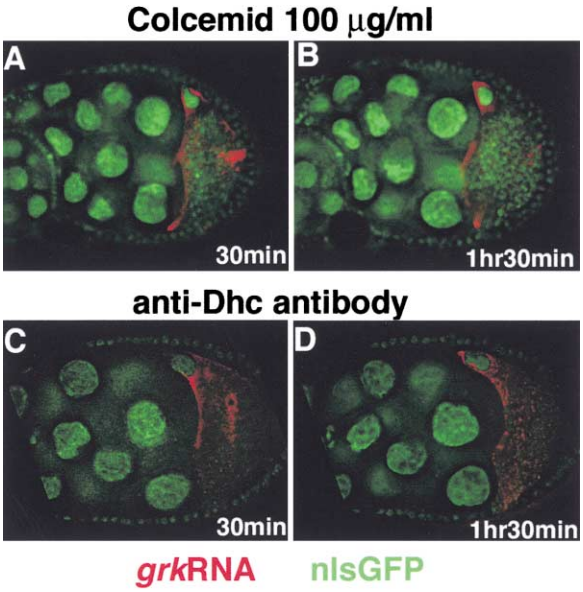

Figure 5. The Second Step of *grk* RNA Localization Requires MTs and Dynein

(A) A stage 9 egg chamber injected with Colcemid (100 μg/ml) approximately 30 min after *grk* RNA injection.

(B) One hour after Colcemid injection, no further localization of *grk* RNA occurs, but the RNA already at the anterior and in the dorsoanterior cap remains localized.

(C) A stage 9 egg chamber injected with anti-Dhc antibody P1H4 30 min after injection with *grk* RNA, which has partly localized to the anterior and near the oocyte nucleus.

(D) One hour after injection of the anti-Dhc, *grk* RNA is still only partly localized.

dhc mutant egg chambers injected with *grk* RNA show localization to a dorsoanterior cap similar to wild-type, 36% show anterior and a weak dorsoanterior localization, and 43% show no localization after 1 hr (n = 14; Figure 4E). We interpret the *dhc* mutants as causing a reduction in the efficiency of Dhc function, while we interpret the anti-Dhc antibody experiments as representing a complete knockout of Dhc function, equivalent to a null allele. We therefore conclude that injected *grk* RNA moves to the anterior using Dynein-dependent transport to the minus ends of MTs.

We were unable to determine the speed of movement of *grk* RNA particles in the *dhc* allelic combinations, as RNA particles appeared to form less readily in the mutant egg chambers than in controls. Instead, to test whether the *grk* RNA particle movement is reduced in *dhc* alleles, we injected *grk* RNA into *dhc* mutant embryos. We found that, in control embryos, the localization of injected *grk* RNA (Figures 5A–5C) was very similar to that of *wg* and pair-rule transcripts previously characterized in embryos (Wilkie and Davis, 2001). Injected *grk* RNA particles localize in control embryos at an average speed of 0.46 ± 0.09 μm/sec (n = 21 particle movements). In two different allelic combinations of *dhc* mutants (dhc^{8-1}/dhc^{6-10} and dhc^{6-6}/dhc^{6-8}), the speed of movement of *grk* particles is reduced to 0.198 ± 0.048 μm/sec (n = 78 particle movements) and 0.19 ± 0.06 μm/sec (n = 82 particle movements), respectively. We conclude that, despite not normally being present in the embryo, *grk* RNA is able to recruit all the machinery required for Dynein-dependent apical localization. These data also strengthen the conclusion that *grk* RNA localizes by a Dynein-dependent mechanism in the oocyte.

To test the dependence of the dorsoanterior movement of *grk* RNA on Dynein, we injected *grk* RNA and waited for approximately 30 min, until the RNA completed most of the first step, and then injected Colcemid or antibodies against Dhc. Either Colcemid (Figures 5D and E) or anti-Dhc (Figures 5F and 5G) injection after completion of the first step does not strongly affect the distribution of RNA that is already localized at the anterior, but the anterior RNA is unable to continue on the second step to the dorsoanterior corner. We interpret these results as follows. Colcemid reduces the length of MTs but does not depolymerize MTs completely. Anteriorly localized RNA (that has completed only the first step) remains bound to the short MTs at the anterior but is unable to move dorsally because the MTs leading to the dorsoanterior corner are also much shortened.

An Anterior Network of MTs Surrounds the Oocyte Nucleus and Contains a High Concentration of MT Minus Ends in a Dorsoanterior Cap

The existence of two distinct MT- and Dynein-dependent steps of *grk* RNA localization in the oocyte suggests that the two steps could involve movement along two distinct MT networks. Previous experiments in stage 9 oocytes do not address this question directly but show that MTs exist in an anteroposterior gradient, with high concentrations in the anterior and low concentrations at the posterior (see Introduction).

To attempt to visualize the different networks of MTs on which the two steps of *grk* RNA localization could occur, we improved the resolution and sensitivity of detection of minus ends of MTs with the Nod-LacZ marker using immunodetection with fluorescent secondary antibodies (see Experimental Procedures), instead of histochemical detection with X-gal staining (Clark et al., 1997). Our results show that there is a concentration of minus ends all over the anterior of the oocyte, as previously reported (Clark et al., 1997), but also a particularly high concentration in a dorsoanterior cap around the nucleus (Figure 6A). Minus ends of MTs are also found along the entire anterior cortex, with lower concentrations in the middle of the anterior "plate" as well as some minus ends at the junction of the follicle cells and oocyte (Figure 6B). Nod-LacZ distribution is therefore different from that of *grk* mRNA, as it is likely to mark all minus ends of MTs, whereas *grk* mRNA mostly localizes at the dorsoanterior cap.

To further study the distinction between *grk* RNA and Nod-LacZ distribution, we crossed the Nod-LacZ marker into a *squid* mutant background (see Experimental Procedures) previously shown to disrupt *grk* mRNA disrtribution (this paper and Norvell et al., 1999). In contrast to *grk* mRNA, Nod-LacZ distribution in *squid* mutants is indistinguishable from that in control egg chambers (data not shown and Figure 6). We conclude that, while Nod-LacZ is a marker for all minus ends of MTs

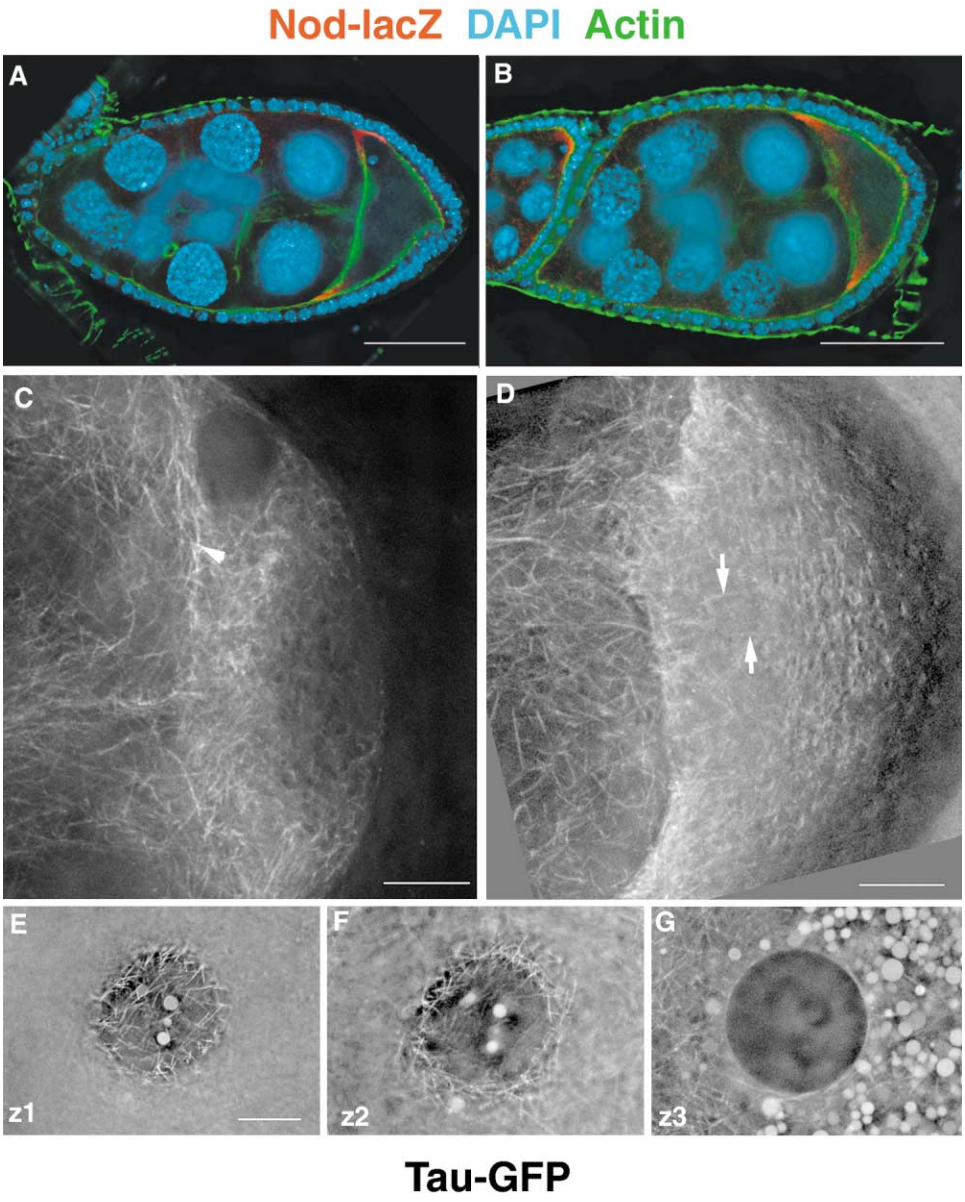

Figure 6. A Network of MTs Is Associated with the Oocyte Nucleus, with MT Minus Ends at a Dorsoanterior Cap

(A–B) Stage 9 Nod-LacZ egg chambers stained with polyclonal anti β-galactosidase antibody visualized by fluorescent secondary antibody (red). Phalloidin-Alexa 488 staining (green) and DAPI staining (cyan) visualize actin and DNA, respectively.

(A) Nod-LacZ, the putative MT minus end marker, is strongly localized at the dorsoanterior cap (where the condensed DNA of the oocyte nucleus can be seen in the DAPI channel) and more weakly in a ventroanterior cap.

(B) Another similar egg chamber orientated with the dorsal side pointing out of the page, showing an anterior cortical ring of Nod-LacZ as well as fainter Nod-LacZ accumulation in the center of the anterior. Note that the red channel is more strongly contrasted in (B) than in (A).

(C–G) Tau-GFP egg chambers revealing MT distribution around the oocyte nucleus and in the anterior region in stage 9 oocytes.

(C) A network of MTs can be visualized surrounding the oocyte nucleus and near the anterior of the oocyte.

(D) A cross-section through the center of a similar Tau-GFP egg chamber revealing some MT arrays deep in the anterior of the oocyte.

(E–G) A high-powered image of three different focal planes (Z1–Z3) of the oocyte nucleus in a Tau-GFP egg chamber (dorsal pointing out of the page). Z2 is 1.5 μm deeper than Z1, and Z3 is 4 μm deeper than Z2. The MTs form a basket around the nucleus (E and F) and extend into the oocyte (G). Note that single MTs are more clearly visible on the surface than in the interior of the oocyte and in the nurse cells that lack the autofluorescence of the yolk. Long segments of MTs are only occasionally visualized, when they lie in the plane of focus ([C], arrowheads; [D], arrows).

in the oocyte, Squid is required for *grk* RNA to localize specifically to a subset of minus ends at the dorsoanterior corner.

We also studied the distribution of MTs in living specimens using the Tau-GFP marker, which decorates MTs, by improving the imaging of MTs near the surface (see

Experimental Procedures) at a higher magnification and resolution than previously described (Januschke et al., 2002; Micklem et al., 1997). A highly convoluted array of MTs exists in the anterior of the oocyte (Figure 6C). Optical sectioning through the nucleus reveals that this anterior array of MTs forms a basket around the oocyte nucleus (Figures 6C and 6E–6G). MTs could also be visualized in the center of the anterior (Figure 6D). These results support, but do not demonstrate conclusively, the existence of two distinct networks of MTs, one forming a basket surrounding the oocyte nucleus, with the MT minus ends at the dorsoanterior cap, and the other with the minus ends at the diffuse anterior MTOC and the plus ends extending toward the posterior. While many MTs appear very short because they do not lie in the plane of observation, some long MTs are observed, which could provide tracks on which *grk* RNA travel anteriorly during the first step, or dorsally during the second step, of localization (Figures 6C and 6D).

Discussion

We have shown that, like *wg* and pair-rule transcripts in the embryo (Bullock and Ish-Horowicz, 2001; Wilkie and Davis, 2001), injected *grk* RNA is able to recruit all the factors required for its correct localization within the cytoplasm of stage 9 oocytes or blastoderm embryos. *grk* RNA assembles into particles that move in two distinct steps within the oocyte to the dorsoanterior corner of the oocyte. The particles first move through the interior of the oocyte to the anterior and then turn and move toward the nucleus and become localized to a dorsoanterior cap. The switch from step one to two occurs most frequently near the anterior, but can also occur in the interior of the oocyte. Both steps of *grk* RNA movement require MTs and Dynein. We propose that the two steps are mechanistically distinct and occur on different networks of MTs.

We have shown that *grk* RNA particle movements in the oocyte are Dynein dependent, as is the apical localization of injected *grk* (this paper), *wg*, and pair-rule RNA particles in the embryo (Wilkie and Davis, 2001). The differences in speeds of particle movements observed in the embryo and oocyte are most likely due to inherent differences in the tissues, rather than an indication of fundamentally different mechanisms of motility. We suggest that the slower speeds of RNA particle movements observed in the oocyte are due to greater frequencies of particle pausing as well as the fact that all known developmental processes are much slower in the oocyte than in the embryo. Furthermore, it is generally accepted that the in vivo speeds of molecular motors can vary considerably from their speeds in vitro because of availability of accessory factors and in vivo regulation.

We were able to study the movement of *grk* RNA only in oocytes whose MTs have already undergone repolarization (stage 8 and later), as injection into the smaller, earlier stages causes a severe disruption of cytoplasmic position and is more difficult to interpret. Nevertheless, we anticipate that, before stage 7, injected *grk* RNA would most likely localize to the posterior, where the minus ends of MTs are located. There are many reasons to think that endogenous *grk* mRNA localization occurs by similar mechanisms to those we have defined for injected *grk* RNA. First, injected and endogenous *grk* RNA localize to very similar sites in the oocyte and are localized to a similar punctate distribution in the dorsoanterior corner. Second, *grk* is the only RNA that is known to localize dorsoanteriorly when injected into the oocyte; others tested localize anteriorly (*K10*) or do not localize (*bcd*, mutant *K10*, and *hb*). Third, injected and endogenous *grk* RNA are mislocalized in precisely the same way in *squid* mutants. Fourth, both injected and endogenous *grk* RNA localization depend on MTs and Dynein (Duncan and Warrior, 2002; Januschke et al., 2002).

It is currently not resolved where *grk* RNA is synthesized. One view is that *grk* is transcribed in the nurse cells, like *bcd* and *osk*, and is subsequently transported into the oocyte (Thio et al., 2000). Another view is that it is transcribed by the oocyte nucleus (Saunders and Cohen, 1999). It seems most likely that *grk* is synthesized at different sites at different times of oogenesis: in early stages, it is synthesized by the nurse cells and, in late stages, by the oocyte nucleus. Whatever the site of synthesis of *grk* RNA, our description of the path of movement and mechanism of movement of injected *grk* RNA is likely to be relevant to endogenous *grk* transcripts. If *grk* is transcribed in the nurse cells, then the two-step movement provides a Dynein-dependent mechanism for delivering *grk* RNA to the dorsoanterior corner from its site of entry into the oocytes. Alternatively, if *grk* RNA is synthesized by the oocyte nucleus, then the same two steps would deliver *grk* RNA to the dorsoanterior corner after export out of the oocyte nucleus.

The Oocyte Contains Distinct Networks of MTs, Each of which Has Its Own Specific Minus Ends

We have analyzed the organization of MTs in the oocyte with high-resolution imaging of Tau-GFP and Nod-LacZ distributions in the oocyte. We detect a particularly high concentration of MT minus ends at the dorsoanterior corner as well as in the anterior cortex and entire anterior. The presence of an MT network associated with the oocyte nucleus explains why a higher concentration of MTs are found in the anterior than in the posterior (Micklem et al., 1997), despite the diffuse nature of the MTOC in the oocyte. A distinct network of MTs associated with the oocyte nucleus also explains why, in *merlin* mutant oocytes, we observed injected *grk* RNA accumulating at the posterior, where the oocyte nucleus is located. We also detect a high concentration of MT minus ends in an anterior ring in addition to a lower concentration all over the anterior. Considering all our results in the context of the previously published data on MT distribution in the oocyte leads us to propose the following model for MT organization in the oocyte (Figure 7). In addition to MTs with their minus ends at the diffuse anterior MTOC (Figure 7, green) and their plus ends at the posterior (Clark et al., 1994, 1997; Micklem et al., 1997), there are some other MTs with their minus ends throughout all parts of the cortex (Figure 7, cyan) (Cha et al., 2001, 2002). We propose that, in addition to these networks, there is also a distinct network of MTs that

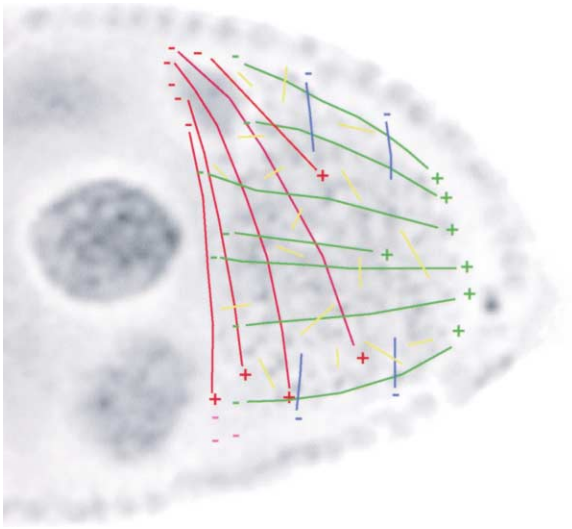

Figure 7. Model for the Organization of MTs in the Oocyte

Four classes of MTs are drawn in red, blue, green, and yellow over a black and white inverted image of an nlsGFP egg chamber. Green MTs have their plus ends at the posterior and minus end all over the anterior; we propose that they are used to transport *grk* RNA during the first step of its localization. Blue MTs have their minus ends at the cortex and are proposed to be used by Kin I to exclude *osk* RNA from the cortex (see text). Red MTs are specifically associated with the oocyte nucleus forming a high concentration of minus ends in the dorsoanterior cap. We propose that only the second step of *grk* localization, but not anterior localization of *bcd* and *K10* RNAs, occurs on these MTs. Yellow MTs have no orientation, and their minus ends occur throughout the entire oocyte. Magenta MT minus ends are part of an array in the anterior.

are specifically associated with the oocyte nucleus (Figure 7, red). These MTs form a loose basket surrounding the nucleus and radiate throughout the anterior and partly into the middle of the oocyte. Our observations of Tau-GFP and previous work (Cha et al., 2001) suggest that there are many other MTs that are more loosely organized throughout much of the oocyte (Figure 7, yellow).

The organization of MTs we propose provides a good explanation for why the *grk* particle movements we observe occur in two distinct steps. We propose that, during the first step of movement of *grk* particles to the anterior of the oocyte, the RNA is likely to be moving on MTs whose plus ends are at the posterior of the oocyte and whose minus ends are along the entire anterior. The second step of movement of the particles is likely to occur on the MT network that forms a basket around the nucleus, with the MT minus ends at the dorsoanterior corner and the plus ends extending toward the anterior and, also, partly into the middle of the oocyte. This model for MT organization fits well with the fact that many *grk* RNA particles were observed to make sharp turns at the anterior, and some in the interior, of the oocyte.

A Model for Sorting Different Transcripts to Distinct Subsets of MT Minus Ends with the Same Dynein Motor

Our model showing that distinct classes of MTs exist within the oocyte begs the question, how does Dynein-dependent transport deliver *grk* RNA to a very different destination from other RNAs in the oocyte, which may also be transported to the minus ends of MTs by Dynein? We propose that different RNAs that are transported to the minus ends of MTs by the same Dynein motors could move on distinct networks of MTs. This would explain why the destination of injected *bcd* RNA (which is thought to require Dynein for its localization [Schnorrer et al., 2000]), depends on whether it is preexposed to nurse cell cytoplasm (Cha et al., 2001). *bcd* RNA injected into the oocyte moves to the nearest cortex along MTs whose minus ends are at the cortex. However, *bcd* RNA that is preexposed to nurse cell cytoplasm is able to move from the posterior to the anterior of the oocyte, apparently in a similar route to that in step 1 of *grk* localization, which we have defined (Cha et al., 2001). Step 2 of *grk* RNA particle movement is not shared with *bcd* RNA and could occur along the MT network that is specifically associated with the oocyte nucleus. Interestingly, *bcd*, but not *grk*, mRNA localization requires γ-Tub37C and Dgrip75 (Schnorrer et al., 2002).

It is most likely that specific transacting factors that recognize RNA signals are responsible for determining which RNAs use which motors and also which distinct MT network is utilized during the Dynein-dependent transport to different destinations. For example, in nerve cells, the choice of cytoplasmic destination of cargo transported by Kinesin is determined by the presence or absence of a protein called GRIP (Setou et al., 2002). Such key transacting factors are likely to also include Squid (Kelley, 1993) and K10 (Cheung et al., 1992), since, in mutants of these genes, *grk* mRNA is localized in the anterior, rather than the dorsoanterior corner (Norvell et al., 1999; Serano et al., 1995). However, in addition to the transacting factors, the different MTs are likely to differ in some way, allowing the different kinds of RNA-motor complexes to distinguish among them. Such differences could include chemical modifications of tubulin or different tubulin isoforms as well as distinct populations of MT-associated proteins (MAPs). It is also possible that γTub37C and Dgrip75 (Schnorrer et al., 2002) could be involved in selectively nucleating a subset of MTs used for *bcd*, but not *grk*, mRNA localization.

Dynein-dependent motility of RNA and other cargo to the minus ends of MTs is likely to be a widely deployed mechanism within cells. Selective utilization of different MT networks would provide a nice way to sort different cellular components that are transported by the same Dynein motor to a variety of distinct minus ends in the same cell. Our rapid and efficient real-time assays for mRNA localization will allow us to begin to define the *cis*-acting signals and *trans*-acting factors that determine which subset of MTs are selected by different RNA cargos that utilize the same motors.

Experimental Procedures

Fly Strains

Stocks were raised on standard cornmeal-agar medium at 25°C. RNA was injected into wild-type (Oregon R) egg chambers or those of a strain with four copies of the nlsGFP transgene (yw; nlsGFPM; nlsGFPN) (Davis et al., 1995) and *sqd*^{1}/*Df(3)urd* (Norvell et al., 1999). *yw, mer*^{ts1} females were dissected after shifting homozygous females to the restrictive temperature for 3 days (MacDougall et al.,

2001) prior to injection. *dhc64C* mutants were from T. Hays (Gepner et al., 1996). The semiviable allelic combinations used ($dhc^{6\text{-}6}/dhc^{6\text{-}12}$) are slightly more severe than the viable allelic combinations of $dhc^{8\text{-}1}/dhc^{6\text{-}10}$ and $dhc^{6\text{-}6}/dhc^{6\text{-}8}$, in which the speed of apical mRNA transport in the blastoderm embryo is reduced (Wilkie and Davis, 2001).

RNA In Situ Hybridization

In situ hybridization was performed as previously described (Wilkie et al., 1999) by fluorescent tyramide detection (NEN LifeSciences). *grk* probes were fragmented in carbonate buffer (Cox et al., 1984) to allow greater probe penetration. Ovaries were prepared for hybridization as described in MacDougall et al. (2001).

Synthesis of Fluorescently Labeled, Capped RNA

RNA was transcribed in vitro as previously described (Wilkie and Davis, 2001) from plasmids containing *grk* cDNA (G. Schüpbach), *hb* cDNA (B. Edgar), *K10 tls* (transport localization signal), or *K10 mutant tls* (R. Cohen and S. Bullock).

Injection of RNA and Inhibitors

Prior to injection, egg chambers were dissected directly onto coverslips in Series 95 halocarbon oil (KMZ Chemicals). Egg chambers were separated into individual ovarioles or egg chambers for injection. Oocytes were microinjected with Femtotip needles (Eppendorf). RNAs were injected at concentrations of 250–500 ng/μl, and Colcemid (Sigma) was injected at concentrations of 100 μg/ml or 30 μg/ml. Anti-Dynein antibodies (T. Hays or D. Sharp) were spot dialyzed as previously described (Wilkie and Davis, 2001).

Immunolocalization of Proteins

Ovaries were dissected and prepared for DAPI, phalloidin, and antibody stainings as previously described (MacDougall et al., 2001), with the following modifications. Ovaries were dissected directly into 3.7% formaldehyde in PBS with 0.1% Triton X and fixed for 20 min. Incubation in a polyclonal rabbit anti β-galactosidase antibody (ICN) at 1:10,000 dilution was performed overnight at 4°C. After three 20 min washes in PBS with 0.1% Triton X, ovaries were incubated with an Alexa Fluor 546-coupled secondary antibody (Molecular Probes) for three hours at room temperature.

Four-Dimensional Imaging and Deconvolution

Fixed egg chambers were mounted in Vectashield (Vector Laboratories). Tau-GFP fluorescence was imaged by placing a breathable membrane (YSI) over the egg chambers after dissection in halocarbon oil on a coverslip, as previously described (Davis, 2000). Imaging was performed on a widefield DeltaVision microscope (Applied Precision) based closely on an original design by John Sedat and David Agard. The microscope consists of an Olympus IX70 inverted microscope with a 12 bit cooled CCD camera (Coolsnap HQ; Roper). Images were acquired with 20×/0.75 NA or 100×/1.4 NA objective lenses selected for symmetric point spread functions and spherical aberration corrected. Out of focus light was reassigned to its point of origin by iterative deconvolution (Davis, 2000). Up to five egg chambers were imaged in parallel, by repeat visiting with a highly accurate XYZ motorized stage.

Particle Tracking

Particles were tracked with a 100×/1.4 NA objective lens and time-lapse intervals of 1 s. Moving particles were manually tracked with DeltaVision (Applied Precision) and Metamorph (Universal Imaging Corporation) image analysis software. The speeds of movement of particles were calculated in micrometers per second according to the distance traveled in each time interval. A vector was taken between the first and last points of each tracked particle to calculate the overall direction of movement. The directions traveled were then calculated with reference to the anteroposterior and dorsoventral axes or the center of the nucleus, as determined by low-magnification imaging in brightfield images or nlsGFP. The directions of movement of particles moving anteriorly and then dorsolaterally were calculated with vectors representing the anterior and lateral phases separately. The directions and speeds of all particles tracked were calculated and plotted with Microsoft Excel. The dorsoanterior phase of the movement toward the nucleus was more difficult to observe, as the particles were spread over a wide range of planes of focus after moving from the site of injection to the anterior of the oocyte. Two approaches were used to identify the dorsoanterior phase of movement. Particles were either injected at the anterior and imaged directly or injected in the center of the oocyte and imaged 20 min later, when they had moved to the anterior. In all cases, particles were analyzed from at least two different egg chambers.

Acknowledgments

We thank David Ish-Horowicz, Catherine Rabouille, Simon Bullock, Isabelle Kos, Veronique Van De Bor, Renald Delanoue, and Hildegard Tekotte for their constructive comments on the manuscript. This work was funded by a Lister Fellowship, a Wellcome Trust Senior Fellowship to I.D., and Darwin Trust, Edinburgh University, and Wellcome Trust studentships to N.M., A.C., and E.M., respectively.

Received: September 16, 2002
Revised: January 10, 2003

References

Bertrand, E., Chartrand, P., Schaefer, M., Shenoy, S.M., Singer, R.H., and Long, R.M. (1998). Localization of ASH1 mRNA particles in living yeast. Mol. Cell *2*, 437–445.

Bobola, N., Jansen, R.P., Shin, T.H., and Nasmyth, K. (1996). Asymmetric accumulation of Ash1p in postanaphase nuclei depends on a myosin and restricts yeast mating-type switching to mother cells. Cell *84*, 699–709.

Brendza, R., Serbus, L., Saxton, W., and Duffy, J. (2002). Posterior localization of Dynein and dorsal-ventral axis formation depend on Kinesin in *Drosophila* oocytes. Curr. Biol. *12*, 1541.

Brendza, R.P., Serbus, L.R., Duffy, J.B., and Saxton, W.M. (2000). A function for kinesin I in the posterior transport of *oskar* mRNA and Staufen protein. Science *289*, 2120–2122.

Bullock, S.L., and Ish-Horowicz, D. (2001). Conserved signals and machinery for RNA transport in *Drosophila* oogenesis and embryogenesis. Nature *414*, 611–616.

Cha, B., Koppetsch, B.S., and Theurkauf, W.E. (2001). In vivo analysis of *Drosophila bicoid* mRNA localization reveals a novel microtubule-dependent axis specification pathway. Cell *106*, 35–46.

Cha, B.J., Serbus, L.R., Koppetsch, B.S., and Theurkauf, W.E. (2002). Kinesin I-dependent cortical exclusion restricts pole plasm to the oocyte posterior. Nat. Cell Biol. *4*, 592–598.

Cheung, H.K., Serano, T.L., and Cohen, R.S. (1992). Evidence for a highly selective RNA transport system and its role in establishing the dorsoventral axis of the Drosophila egg. Development *114*, 653–661.

Clark, I., Giniger, E., Ruohola-Baker, H., Jan, L.Y., and Jan, Y.N. (1994). Transient posterior localization of a kinesin fusion protein reflects anteroposterior polarity of the *Drosophila* oocyte. Curr. Biol. *4*, 289–300.

Clark, I.E., Jan, L.Y., and Jan, Y.N. (1997). Reciprocal localization of Nod and kinesin fusion proteins indicates microtubule polarity in the *Drosophila* oocyte, epithelium, neuron and muscle. Development *124*, 461–470.

Cox, K.H., DeLeon, D.V., Angerer, L.M., and Angerer, R.C. (1984). Detection of mRNAs in sea urchin embryos by in situ hybridization using asymmetric RNA probes. Dev. Biol. *101*, 485–502.

Davis, I. (2000). Visualising fluorescence in *Drosophila*—optimal detection in thick specimens. In Protein Localisation by Fluorescence Microscopy: A Practical Approach, V.J. Allan, ed. (Oxford: OUP), pp. 131–162.

Davis, I., Girdham, C.H., and O'Farrell, P.H. (1995). A nuclear GFP that marks nuclei in living *Drosophila* embryos—maternal supply overcomes a delay in the appearance of zygotic fluorescence. Dev. Biol. *170*, 726–729.

Davis, I., and Ish-Horowicz, D. (1991). Apical localization of pair-rule transcripts requires 3′ sequences and limits protein diffusion in the *Drosophila* blastoderm embryo. Cell *67*, 927–940.

Driever, W., and Nüsslein-Volhard, C. (1988). A gradient of bicoid protein in *Drosophila* embryos. Cell *54*, 83–93.

Duncan, J.E., and Warrior, R. (2002). The cytoplasmic Dynein and Kinesin motors have interdependent roles in patterning the *Drosophila* oocyte. Curr. Biol. *12*, 1982–1991.

Ephrussi, A., Dickinson, L.K., and Lehmann, R. (1991). Oskar organizes the germ plasm and directs localization of the posterior determinant nanos. Cell *66*, 37–50.

Erdelyi, M., Michon, A.M., Guichet, A., Glotzer, J.B., and Ephrussi, A. (1995). Requirement for *Drosophila* cytoplasmic tropomyosin in *oskar* mRNA localization. Nature *377*, 524–527.

Gepner, J., Li, M., Ludmann, S., Kortas, C., Boylan, K., Iyadurai, S.J., McGrail, M., and Hays, T.S. (1996). Cytoplasmic dynein function is essential in *Drosophila* melanogaster. Genetics *142*, 865–878.

Glotzer, J.B., Saffrich, R., Glotzer, M., and Ephrussi, A. (1997). Cytoplasmic flows localize injected *oskar* RNA in *Drosophila* oocytes. Curr. Biol. *7*, 326–337.

Gonzalez-Reyes, A., Elliott, H., and St Johnston, D. (1995). Polarization of both major body axes in *Drosophila* by Gurken-Torpedo signaling. Nature *375*, 654–658.

Gonzalez-Reyes, A., and St Johnston, D.S. (1998). Patterning of the follicle cell epithelium along the anterior-posterior axis during *Drosophila* oogenesis. Development *125*, 2837–2846.

Jansen, R.P. (2001). mRNA localization: message on the move. Nat. Rev. Mol. Cell Biol. *2*, 247–256.

Jansen, R.P., Dowzer, C., Michaelis, C., Galova, M., and Nasmyth, K. (1996). Mother cell-specific HO expression in budding yeast depends on the unconventional myosin myo4p and other cytoplasmic proteins. Cell *84*, 687–697.

Januschke, J., Gervais, L., Dass, S., Kaltschmidt, J.A., Lopez-Schier, H., Johnston, D.S., Brand, A.H., Roth, S., and Guichet, A. (2002). Polar transport in the *Drosophila* oocyte requires Dynein and Kinesin I cooperation. Curr. Biol. *12*, 1971–1981.

Kelley, R.L. (1993). Initial organization of the Drosophila dorsoventral axis depends on an RNA-binding protein encoded by the *squid* gene. Genes Dev. *7*, 948–960.

King, S.J., and Schroer, T.A. (2000). Dynactin increases the processivity of the cytoplasmic dynein motor. Nat. Cell Biol. *2*, 20–24.

Kloc, M., Zearfoss, N.R., and Etkin, L.D. (2002). Mechanisms of subcellular mRNA localization. Cell *108*, 533–544.

Lall, S., Francis-Lang, H., Flament, A., Norvell, A., Schupbach, T., and Ish-Horowicz, D. (1999). Squid hnRNP protein promotes apical cytoplasmic transport and localization of *Drosophila* pair-rule transcripts. Cell *98*, 171–180.

Lipshitz, H.D., and Smibert, C.A. (2000). Mechanisms of RNA localization and translational regulation. Curr. Opin. Genet. Dev. *10*, 476–488.

Long, R.M., Gu, W., Lorimer, E., Singer, R.H., and Chartrand, P. (2000). She2p is a novel RNA-binding protein that recruits the Myo4p-She3p complex to ASH1 mRNA. EMBO J. *19*, 6592–6601.

MacDougall, N., Lad, Y., Wilkie, G., Francis-Lang, H., Sullivan, W., and Davis, I. (2001). Merlin, the *Drosophila* homologue of Neurofibromatosis-2, is specifically required in posterior follicle cells for axis formation in the oocyte. Development *128*, 665–673.

Micklem, D.R., Dasgupta, R., Elliott, H., Gergely, F., Davidson, C., Brand, A., Gonzalez-Reyes, A., and St Johnston, D. (1997). The *mago nashi* gene is required for the polarisation of the oocyte and the formation of perpendicular axes in *Drosophila*. Curr. Biol. *7*, 468–478.

Munchow, S., Sauter, C., and Jansen, R.P. (1999). Association of the class V myosin Myo4p with a localised messenger RNA in budding yeast depends on She proteins. J. Cell Sci. *112*, 1511–1518.

Neuman-Silberberg, F.S., and Schüpbach, T. (1993). The *Drosophila* dorsoventral patterning gene *gurken* produces a dorsally localized RNA and encodes a TGF alpha-like protein. Cell *75*, 165–174.

Nilson, L.A., and Schüpbach, T. (1999). EGF receptor signaling in *Drosophila* oogenesis. Curr. Top. Dev. Biol. *44*, 203–243.

Norvell, A., Kelley, R.L., Wehr, K., and Schüpbach, T. (1999). Specific isoforms of Squid, a *Drosophila* hnRNP, perform distinct roles in *gurken* localization during oogenesis. Genes Dev. *13*, 864–876.

Palacios, I.M., and Johnston, D.S. (2001). Getting the message across: the intracellular localization of mRNAs in higher eukaryotes. Annu. Rev. Cell Dev. Biol. *17*, 569–614.

Palacios, I.M., and Johnston, D.S. (2002). Kinesin light chain-independent function of the Kinesin heavy chain in cytoplasmic streaming and posterior localisation in the Drosophila oocyte. Development *129*, 5473–5485.

Pokrywka, N.J., and Stephenson, E.C. (1991). Microtubules mediate the localization of *bicoid* RNA during *Drosophila* oogenesis. Development *113*, 55–66.

Saunders, C., and Cohen, R.S. (1999). The role of oocyte transcription, the 5′UTR, and translation repression and derepression in *Drosophila gurken* mRNA and protein localization. Mol. Cell *3*, 43–54.

Schnorrer, F., Bohmann, K., and Nüsslein-Volhard, C. (2000). The molecular motor dynein is involved in targeting swallow and *bicoid* RNA to the anterior pole of *Drosophila* oocytes. Nat. Cell Biol. *2*, 185–190.

Schnorrer, F., Luschnig, S., Koch, I., and Nusslein-Volhard, C. (2002). γ-*Tubulin37C* and γ-*tubulin ring complex protein 75* are essential for *bicoid* RNA Localization during *Drosophila* oogenesis. Dev. Cell *3*, 685–696.

Serano, T.L., and Cohen, R.S. (1995). A small predicted stem-loop structure mediates oocyte localization of Drosophila K10 mRNA. Development *121*, 3809–3818.

Serano, T.L., Karlin-McGinness, M., and Cohen, R.S. (1995). The role of fs(1)K10 in the localization of the mRNA of the TGF alpha homolog gurken within the *Drosophila* oocyte. Mech. Dev. *51*, 183–192.

Setou, M., Seog, D.H., Tanaka, Y., Kanai, Y., Takei, Y., Kawagishi, M., and Hirokawa, N. (2002). Glutamate-receptor-interacting protein GRIP1 directly steers kinesin to dendrites. Nature *417*, 83–87.

St Johnston, D., Driever, W., Berleth, T., Richstein, S., and Nüsslein-Volhard, C. (1989). Multiple steps in the localization of bicoid RNA to the anterior pole of the *Drosophila* oocyte. Development *107*, 13–19.

Takizawa, P.A., and Vale, R.D. (2000). The myosin motor, Myo4p, binds Ash1 mRNA via the adapter protein, She3p. Proc. Natl. Acad. Sci. USA *97*, 5273–5278.

Tekotte, H., and Davis, I. (2002). Intracellular mRNA localization: motors move messages. Trends Genet. *18*, 636–642.

Theurkauf, W.E., and Hazelrigg, T.I. (1998). In vivo analyses of cytoplasmic transport and cytoskeletal organization during *Drosophila* oogenesis: characterization of a multi-step anterior localization pathway. Development *125*, 3655–3666.

Theurkauf, W.E., Smiley, S., Wong, M.L., and Alberts, B.M. (1992). Reorganization of the cytoskeleton during *Drosophila* oogenesis—implications for axis specification and intercellular transport. Development *115*, 923–936.

Thio, G.L., Ray, R.P., Barcelo, G., and Schüpbach, T. (2000). Localization of gurken RNA in *Drosophila* oogenesis requires elements in the 5′ and 3′ regions of the transcript. Dev. Biol. *221*, 435–446.

van Eeden, F., and St Johnston, D. (1999). The polarisation of the anterior-posterior and dorsal-ventral axes during *Drosophila* oogenesis. Curr. Opin. Genet. Dev. *9*, 396–404.

Vanzo, N.F., and Ephrussi, A. (2002). Oskar anchoring restricts pole plasm formation to the posterior of the *Drosophila* oocyte. Development *129*, 3705–3714.

Wilhelm, J.E., Mansfield, J., Hom-Booher, N., Wang, S., Turck, C.W.,

Hazelrigg, T., and Vale, R.D. (2000). Isolation of a ribonucleoprotein complex involved in mRNA localization in *Drosophila* oocytes. J. Cell Biol. *148*, 427–440.

Wilkie, G.S., and Davis, I. (2001). *Drosophila wingless* and pair-rule transcripts localize apically by dynein-mediated transport of RNA particles. Cell *105*, 209–219.

Wilkie, G.S., Shermoen, A.W., O'Farrell, P.H., and Davis, I. (1999). Transcribed genes are localized according to chromosomal position within polarized *Drosophila* embryonic nuclei. Curr. Biol. *9*, 1263–1266.